ACS Medicinal Chemistry Letters

pubs.acs.org/acsmedchemlett Letter

DNA-Model-Based Design and Execution of Some Fused Benzodiazepine Hybrid Payloads for Antibody−Drug Conjugate Modality

Prasanna Sivaprakasam,* Ivar McDonald, Christiana Iwuagwu, Naidu S. Chowdari, Kevin M. Peese, David R. Langley, Heng Cheng, Michael R. Luzung, Michael A. Schmidt, Bin Zheng, Yichen Tan, Patricia Cho, Souvik Rakshit, Thirumalai Lakshminarasimhan, Sivakrishna Guturi, Kishorekumar Kanagavel, Umamaheswararao Kanusu, Ankita G. Niyogi, Somprabha Sidhar, Rajappa Vaidyanathan, Martin D. Eastgate, Srikanth Kotapati, Madhura Deshpande, Chin Pan, Pina M. Cardarelli, Chunshan Xie, Chetana Rao, Patrick Holder, Ganapathy Sarma, Gregory Vite, and Sanjeev Gangwar

Cite This: *ACS Med. Chem. Lett.* 2021, 12, 404−412 Read Online

ACCESS | Metrics & More | Article Recommendations | Supporting Information

ABSTRACT: A new series with the tetrahydroisoquinoline-fused benzodiazepine (TBD) ring system combined with the surrogates of (1-methyl-1*H*-pyrrol-3-yl)benzene ("MPB") payloads were designed and executed for conjugation with a monoclonal antibody for anticancer therapeutics. DNA models helped in rationally identifying modifications of the "MPB" binding component and guided structure−activity relationship generation. This hybrid series of payloads exhibited excellent *in vitro* activity when tested against a panel of various cancer cell lines. One of the payloads was appended with a lysosome-cleavable peptide linker and conjugated with an anti-mesothelin antibody via a site-specific conjugation method mediated by the enzyme bacterial transglutaminase (BTGase). Antibody−drug conjugate (ADC) **50** demonstrated good plasma stability and lysosomal cleavage. A single intravenous dose of ADC **50** (5 or 10 nmol/kg) showed robust efficacy in an N87 gastric cancer xenograft model.

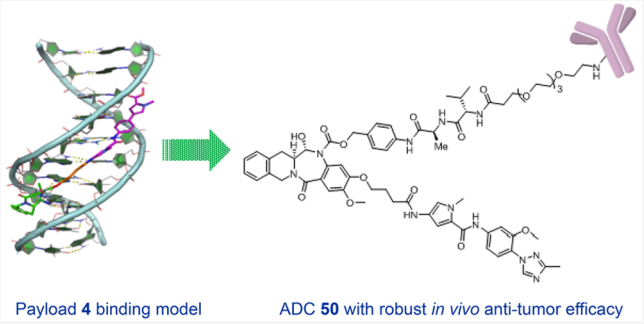

KEYWORDS: *PBD, DNA minor groove binders, DNA binding models, ADC, cytotoxicity*

Antibody−drug conjugates (ADCs) have ascended as powerful biologics that combine the high affinity and specificity of monoclonal antibodies (mAbs) with the promising antitumor efficacy of the payloads.[1,2] Over the last two decades, ADCs have continued to evolve as an attractive modality for the treatment of hematological malignancies and solid tumors.[3] Currently, there are nine approved and marketed ADCs.[4] A cytotoxic agent, often called a payload, that is generally too toxic for systemic administration is combined with mAbs with the help of linkers to specifically target tumor cells. On the basis of the mechanism of action, payloads fall into three categories: antimitotic, DNA-interacting, and transcription-inhibiting. The antimitotic class of payloads used in ADCs act by interacting with tubulin and include maytansinoids, auristatins, tubulysins, and many others.[5] The DNA-interacting class includes calicheamicin, duocarmycin, etc.[6] The transcription inhibitors include amatoxins that bind to RNA polymerase II.[7] Antimitotic and DNA-interacting payloads are most broadly used in ADCs. DNA-interacting agents act by binding to the minor groove and lead to intercalation, scission, alkylation, or cross-linking of strands. Hence, they are also called DNA minor groove binders (MGBs). Another important class of payloads used in ADCs is camptothecins.[8] Camptothecin and its derivatives bind to the topoisomerase I/DNA complex as their mechanism of action.[9]

One of the MGBs that is highly pursued in the ADC architecture is the pyrrolo[2,1-*c*][1,4]benzodiazepine (PBD) class of compounds (Figure 1, example payload **1**).[10−17] PBD dimers bind in the minor groove of DNA, where they form interstrand cross-links with guanines. Rahman et al.[18] reported that some non-covalent heteroaryl pharmacophores have a strong preference for GC-rich DNA sequences either alone or

Received: October 31, 2020
Accepted: January 27, 2021
Published: February 10, 2021

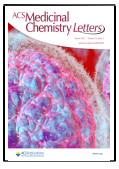

https://dx.doi.org/10.1021/acsmedchemlett.0c00578
ACS Med. Chem. Lett. 2021, 12, 404−412

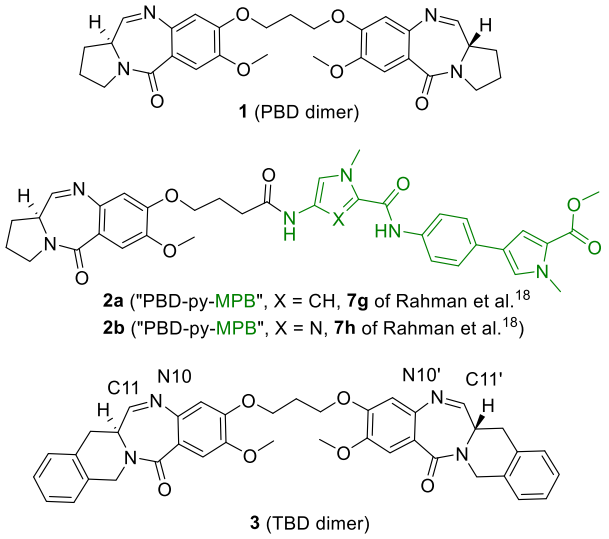

Figure 1. Example structures of PBD dimer,[17] "PBD-py-MPB",[18] and TBD dimer.[19−21]

when combined with PBDs. Compounds **2a** and **2b** are the two most advanced candidates from Rahman et al.[18] Notably, **2b** demonstrated significant antitumor efficacy in breast (MDA-MB-231) and pancreatic (MIA PaCa-2) xenograft models.[18]

As part of our ADC discovery efforts[19−21] and inspired by the report by Rahman et al.,[18] we sought to pursue PBD−4-(1-methyl-1*H*-pyrrol-3-yl)benzeneamine ("MPB" as termed by Rahman et al.[18]) hybrid payloads for the ADC modality (Figure 1, example payloads **2a** and **2b**). The inherent toxicity of these payloads to normal cells motivated us to prosecute these agents for a targeted therapeutic approach like ADC. Our prior experience with PBD molecules led us to hypothesize that some examples in this class might be too potent to achieve an acceptable therapeutic index. An appealing aspect of these hybrid molecules was the potential to tune the properties by preparing a diverse set of analogues through variation of the MPB portion of the molecules. We pursued the reported "PBD−MPB" hybrid payloads in the context of our fused benzodiazepine with a tetrahydroisoquinoline ring system, herein called TBD (Figure 1, example payload **3**).

For benchmarking purposes, we made **4** and **5**, which are the TBD versions of **2a** and **2b**, respectively, from the original publication by Rahman et al.[18] Initial characterization of the payloads was based on an *in vitro* evaluation against a suite of cellular proliferation assays for lung (H226), gastric (N87), ovarian (OVCAR3), and colon (HCT116) cancer cell lines as described in our recent publication.[22] Compounds **4** and **5** showed quite potent (single- to double-digit and subpicomolar) activities in these cell lines (Table 1). A double-stranded B-DNA binding model for **4** was generated using the sequence 5′-AAGAAGGCAA-3′, as reported by Rahman et al.[18] We hypothesized that **4**, which is a TBD variant of **2a**, would also bind to the 5′-AAGAAGGCAA-3′ sequence that was demonstrated to be the preferred binding sequence for **2b**.[18] Figure 2A,B illustrates the binding mode of **4** in the DNA minor groove. The C11−N10 imine of TBD makes a covalent bond with the exocyclic amine of G3 of the DNA, while the "py-MPB" portion of the payload makes non-covalent interactions and nicely follows the curvature of the DNA minor groove.

The DNA-binding model of **4** revealed opportunities to modify the "MPB" portion of the payloads. A set of internally available anilines was evaluated to rationally replace the "MPB" moiety. Among these, we envisioned a (methyltriazolo)benzene replacement (compound **6**) for the "MPB" moiety. We hypothesized that the flat (methyltriazolo)benzene group would nicely complement the minor groove, with one of the ring nitrogens in the triazole ring being in close proximity to the exocyclic amine of G7 in the DNA model to engage in a hydrogen-bonding interaction dynamically. While the H226 cell line activity was retained or improved in **6** compared with its progenitor **4**, the other three cell lines showed diminished activity, with the worst being the OVCAR3 cell line. Compound **7** was made to explore the impact of removing the methyl group in the triazole ring, and it turned out to be equipotent to its methyl counterpart in the H226, N87, and HCT116 cell lines and ∼3-fold more potent in the OVCAR3 cell line. As an N-linked imidazole derivative, **8** lacks the hydrogen-bond acceptor close to the exocyclic amine of G7 and showed a considerable loss of activity across all four cell lines compared with **6**. C-linked imidazole **9** had further-diminished activities across all four cell lines. The substantial drop in the activity is perhaps partly due to the possibility of tautomerization where hydrogen bonding with the exocyclic amine of G7 is absent in one set of tautomers. The perturbed coplanarity between the two terminal rings may also play a role in reducing the activity. For oxazole **10**, which has the ring nitrogen to complement the exocyclic amine of G7, the activity was restored in all of the cell lines except H226 compared to its triazole counterpart **6**.

Next, we kept the methyltriazolo ring constant and surveyed the structure−activity relationship (SAR) around the N-linked phenyl group. *o*-Fluoro analogue **11** showed comparable activity in the H226 cell line and improved activities in the other three cell lines relative to **6**. Slightly bulky ortho substituents negatively impacted the activities in all four cell lines (compounds **12**−**16**). *o*-Hydroxy analogue **17** showed activities comparable to those of **6** in the H226 and HCT116 cell lines. Pyridyl derivative **18** showed an enhancement in activity in the N87 cell line relative to its phenyl counterpart **7**. Compound **19** with a difluoromethyl group instead of the methyl group in **13** showed an improvement in the activities in the N87 and OVCAR3 cell lines. Desmethyl analogue **20** showed a modest drop in activity across all of the tested cell lines except N87 compared with its parent analogue **13**. Dimethyl derivative **21** exhibited a dramatic loss in the activities across all four cell lines, likely hinting at the need for coplanarity of the distal biaryl ring system. We revisited N-linked imidazole (*cf.* compound **8**) and introduced substitutions in the linking phenyl and terminal imidazole rings. Compounds **22**−**26** are the outcomes of this effort, and the combination of chloroimidazole with either a fluorophenyl or pyridine linking ring yielded acceptable activity profiles in all four cell lines. *N*-Phenylpyrazole **27** showed double-digit picomolar activities in three of the four cell lines.

Tricyclic analogues **28** and **29** showed activity profiles comparable to that of **6**. Tricyclic derivative **30** is not as flat as **28** and **29** and showed a marked drop in activities across all four cell lines. Tricyclic analogue **31** exhibited further-diminished activities in all four cell lines. While all three rings in the tricyclic ring system in **30** fit well in the minor groove of the DNA model, the morpholinotriazole portion of the tricyclic ring system in **31** projected outside the minor groove. Aza-*N*-methylbenzimidazole **32** had activities in the single-digit nanomolar range in all four cell lines, which once again may partly be due to the putative suboptimal fit of the bicyclic ring in the minor groove of the DNA.

https://dx.doi.org/10.1021/acsmedchemlett.0c00578
ACS Med. Chem. Lett. 2021, 12, 404−412

Table 1. Compounds and Cytotoxicity Data (IC_{50} in nM)

Compound	Structure	H226	N87	OVCAR3	HCT116
4	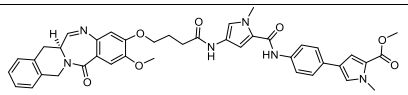	0.006[a]	0.007[a]	0.019[a]	0.003[a]
5	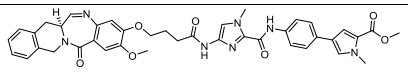	0.018[b]	<0.004[b]	0.045[b]	<0.004[b]
6	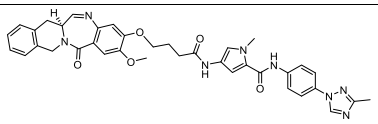	<0.004[a]	0.023[a]	0.135[a]	0.016[a]
7	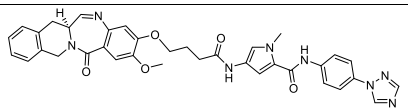	<0.004[b]	0.025[a]	0.042[a]	0.015[a]
8	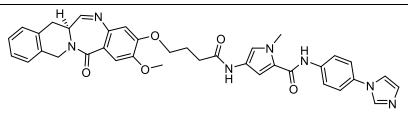	0.178[b]	0.241[b]	0.907[b]	0.088[b]
9	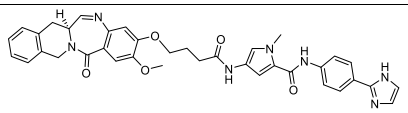	0.659[b]	0.372[b]	0.756[b]	0.104[b]
10	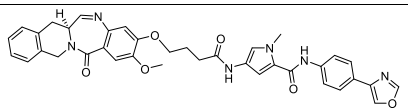	0.025[a]	0.025[a]	0.054[a]	0.010[a]
11	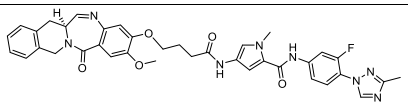	0.007[b]	0.006[b]	0.013[b]	<0.004[b]
12	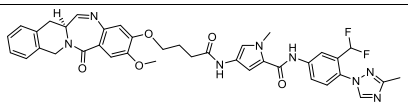	0.053[b]	0.035[b]	0.120[b]	0.039[b]
13	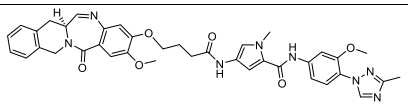	0.028[a]	0.089[a]	0.103[a]	0.022[a]
14	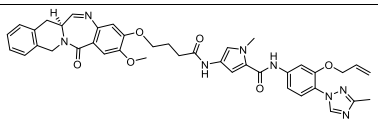	0.067[b]	0.018[a]	0.123[a]	0.023[a]
15	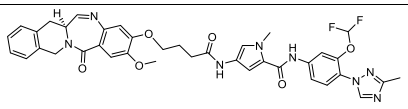	0.060[b]	0.027[b]	0.074[b]	0.023[b]
16	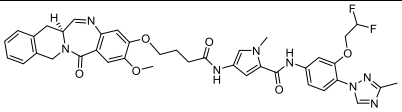	0.099[b]	0.116[b]	0.102[b]	0.026[b]
17	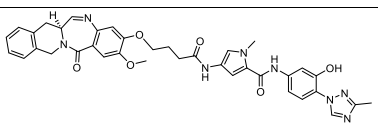	<0.004[a]	0.086[a]	0.386[a]	0.019[a]

https://dx.doi.org/10.1021/acsmedchemlett.0c00578
ACS Med. Chem. Lett. 2021, 12, 404−412

Table 1. continued

Compound	Structure	H226	N87	OVCAR3	HCT116
18	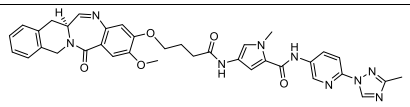	<0.004[b]	0.008[a]	0.034[a]	0.011[a]
19	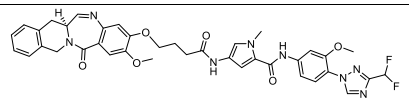	0.018[b]	0.026[b]	0.037[b]	0.014[b]
20	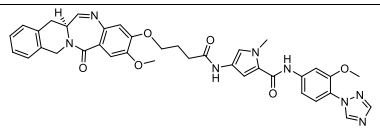	0.104[b]	0.042[b]	0.161[b]	0.041[b]
21	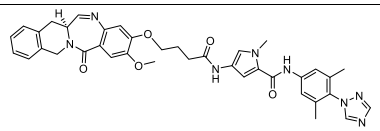	0.682[a]	0.204[a]	0.383[a]	0.185[a]
22	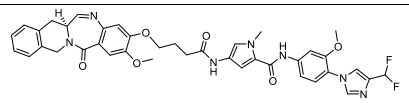	0.112[b]	0.053[b]	0.196[b]	0.055[b]
23	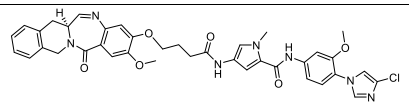	0.105[b]	0.046[b]	0.233[b]	0.038[b]
24	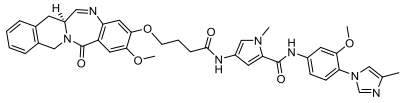	0.186[b]	0.091[b]	0.355[b]	0.057[b]
25	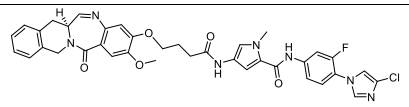	0.032[b]	0.014[b]	0.103[b]	0.027[b]
26	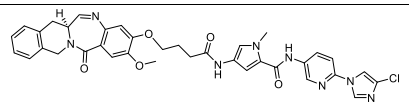	0.019[b]	0.073[b]	0.024[b]	0.018[b]
27	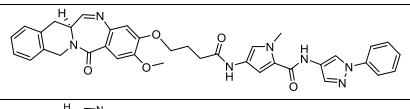	0.030[a]	0.047[a]	0.107[a]	0.012[a]
28	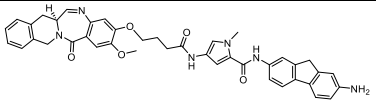	<0.004[a]	0.008[a]	0.028[a]	0.001[b]
29	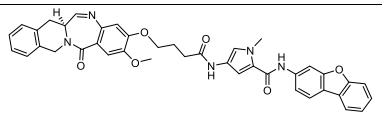	<0.004[a]	0.020[b]	0.065[a]	0.006[b]
30	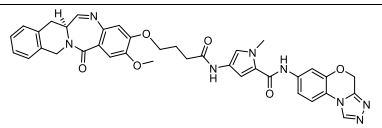	0.239[a]	0.260[a]	0.932[a]	0.078[a]
31	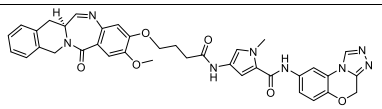	2.46[a]	0.405[a]	1.52[a]	0.285[a]
32	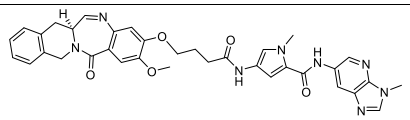	1.20[b]	2.00[a]	3.58[a]	1.37[a]

[a]The IC_{50} value was the result of multiple determinations ($n \geq 2$). [b]The IC_{50} value was obtained after single determination ($n = 1$).

https://dx.doi.org/10.1021/acsmedchemlett.0c00578
ACS Med. Chem. Lett. 2021, 12, 404−412

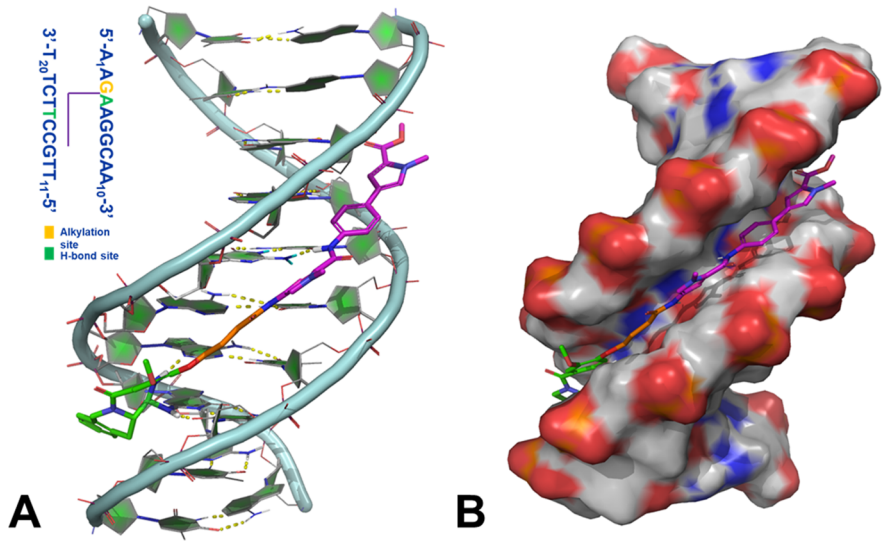

Figure 2. (A) Binding model of **4** in double-helical B-DNA. The inset shows the sequence used in the DNA model development. (B) Surface representation of the DNA model showing the snug fit of **4** in the minor groove. Hydrogen bonds are represented by yellow dotted lines. The covalently bound TBD portion of the payload, the linker, and the non-covalently bound "py-MPB" portion are shown in green, orange, and magenta, respectively. The figure was prepared using PyMOL (The PyMOL molecular graphics system, Version 2.3.0, Schrödinger, LLC).

Scheme 1. Synthetic Route for 4−32

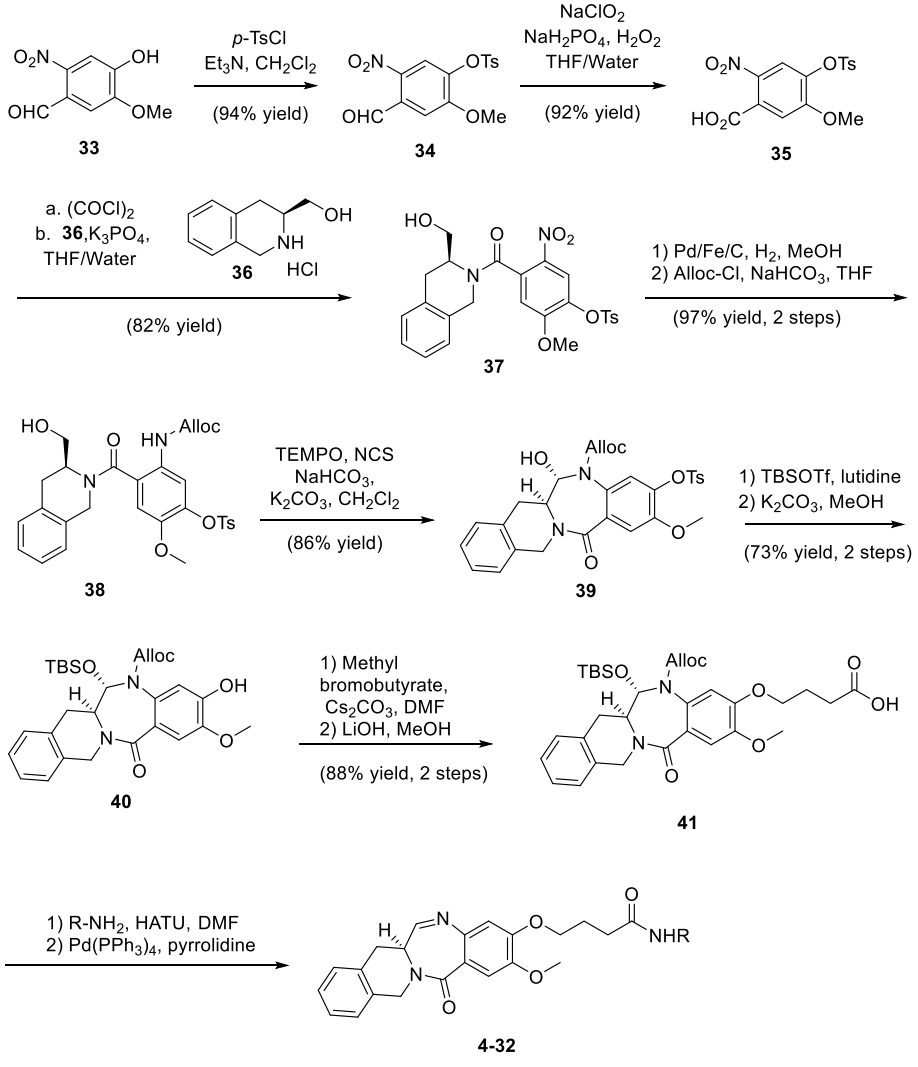

https://dx.doi.org/10.1021/acsmedchemlett.0c00578
ACS Med. Chem. Lett. 2021, 12, 404−412

Scheme 2. Synthetic Route for Payload−Linker 49

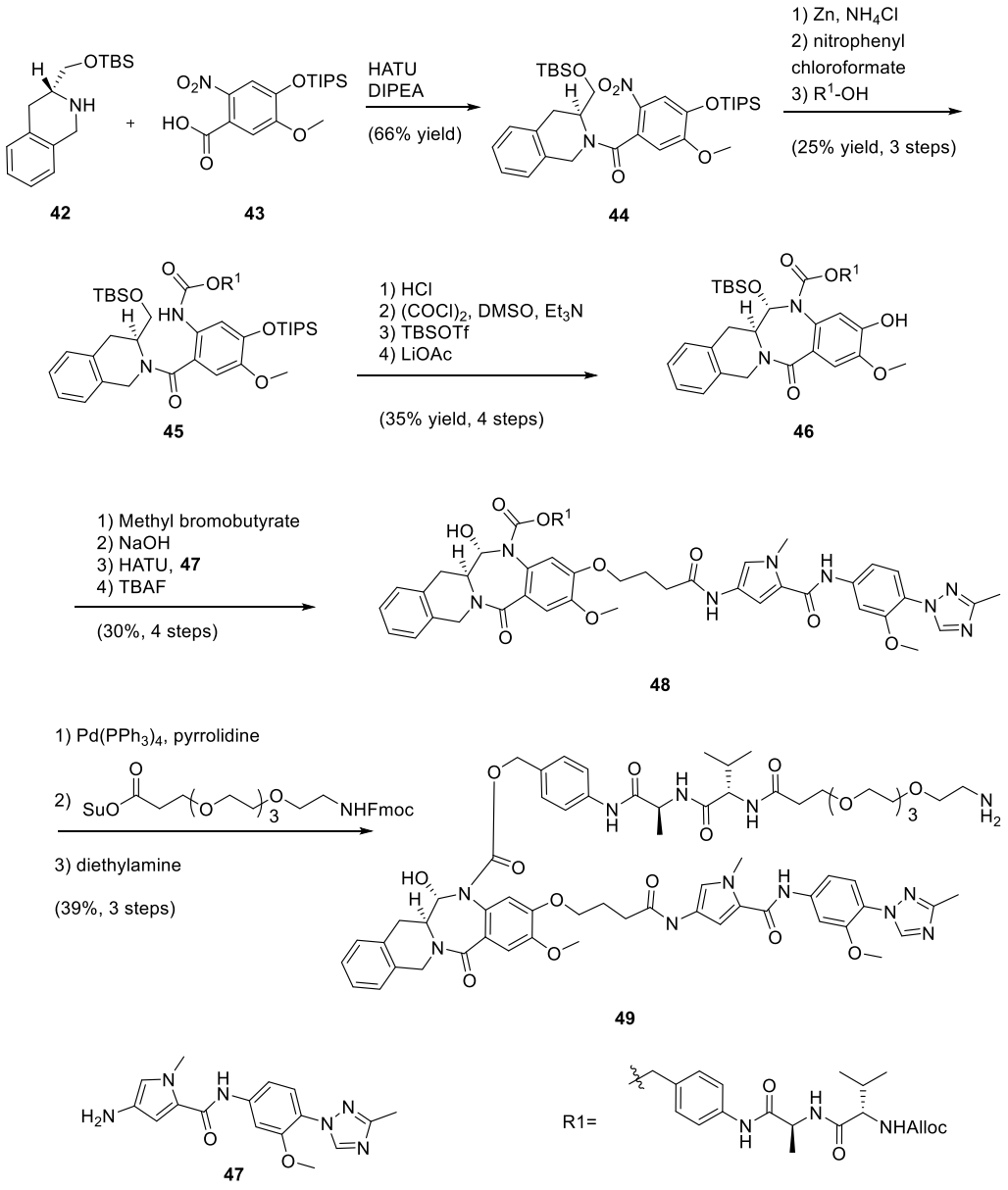

The synthetic route for payloads **4** to **32** is shown in Scheme 1 (see the Supporting Information for details). An effort was started to produce a fit-for-purpose synthetic route capable of delivering tens to hundreds of grams of monomer precursors. This was undertaken to supply ample quantities of material for SAR studies while also providing a blueprint toward a large-scale process. The route begins with aldehyde **33**, obtained from vanillin in three steps, all conducted in continuous flow mode.[23] The phenol was protected as a tosyl ester, which imparted crystallinity to many of the early-stage intermediates and greatly reduced the number of purifications by chromatography. Aldehyde **34** was oxidized to the acid through a Pinnick oxidation (92%), and through the intermediacy of the acid chloride, the acid was coupled with tetrahydroisoquinoline **36** to give amide **37** (82%) under Schotten−Baumann conditions. The nitro group of **37** was reduced with hydrogen gas catalyzed by palladium on carbon doped with 1% iron (99%). The aniline was protected as an allyloxycarbamate (Alloc), again under Schotten−Baumann conditions (98%). Freshly distilled Alloc-Cl was found to eliminate the formation of urea-like byproducts that formed from old lots of Alloc-Cl. The primary alcohol of **38** was oxidized with TEMPO/NCS to afford the aldehyde, which cyclized in situ to form tetracycle **39** as a single aminal diastereomer (86%). We found this to be a strategic place to store bulk material, as it is the last crystalline intermediate in the synthesis. The aminal oxygen in **39** was protected as a TBS ether (89%), and then the tosyl group was removed under the action of potassium carbonate in methanol (82%) to afford phenol **40**, which was then alkylated with methyl bromobutyrate and hydrolyzed to afford key intermediate acid **41** in a robust, scalable 10-step process. This acid was then diversified by amide bond formation followed by deprotection of the Alloc group, which led to spontaneous elimination of the protected hemiaminal, affording the imine products **4**−**32**. It was felt that unmasking the imine functionality as late as possible was important to minimize any potential stability concerns with the potentially reactive imine and also, for safety reasons, to

https://dx.doi.org/10.1021/acsmedchemlett.0c00578
ACS Med. Chem. Lett. 2021, 12, 404−412

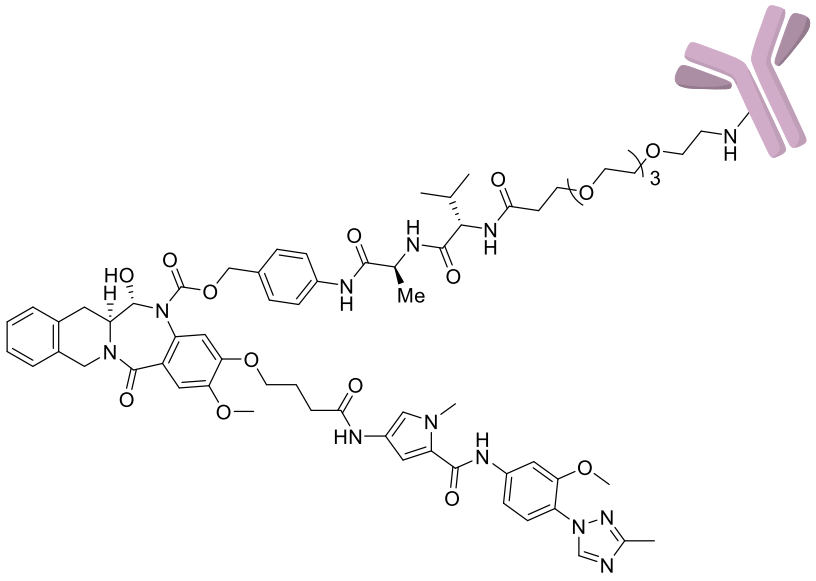

Figure 3. Structure of ADC **50**.

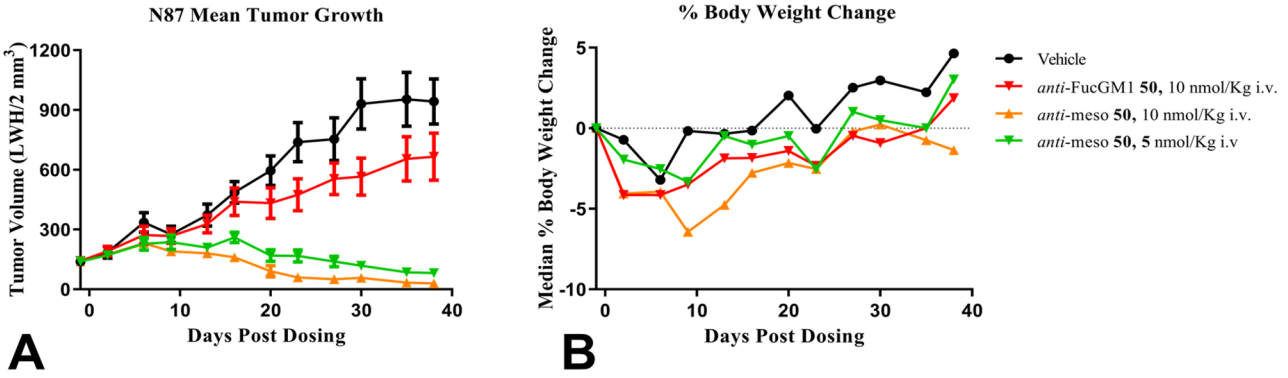

Figure 4. Antitumor efficacy was measured in an established N87 human gastric cancer xenograft model in mice. (A) Time course of tumor volume after administration of a single iv dose of anti-mesothelin-ADC **50**. (B) Time course of median percent body weight change from the same experiment. A dose of 5 or 10 nmol/kg is equivalent to 0.4 or 0.8 mg/kg, respectively.

minimize the number of steps that required handling of these potently cytotoxic compounds.

On the basis of our *in vitro* cytotoxicity SAR and the desired physicochemical properties, **13** was selected as an exemplar for installing the linker for conjugation with an antibody since this starting point might lead us to tune potency up or down if we found the corresponding ADC to be either not potent enough or too poorly tolerated. This synthesis commenced in a manner similar to that of **4**–**32**, albeit on a differentially protected scaffold (Scheme 2). Amide coupling between chiral amine **42** and acid **43** afforded nitro–amide **44**, which was next reduced to the corresponding aniline, and the cathepsin-cleavable valine–alanine–benzyl carbamate linker was installed to give **45**. Cleavage of the TBS ether, oxidation to the hemiaminal, and a subsequent protecting-group manipulation led to phenol **46**, from which the MGB motif was added, similarly to the nonconjugated analogues, to afford **48**. Removal of the Alloc protecting group on the linker followed by installation of a poly(ethylene glycol) 4 (PEG4) spacer gave linker–payload **49**. Conjugation to an antibody that targets the mesothelin[24] antigen using site-specific conjugation mediated by BTGase[25] as described in the Supporting Information provided ADC **50** (Figure 3). The final purified ADC **50** was >98% monomer with a drug to antibody ratio (DAR) of 2.0.

ADC **50** was incubated with cathepsin B at 37 °C for 4 h to check whether this ADC could be cleaved enzymatically by a lysosomal protease. Cleavage of 98% of the payload occurred within 4 h. ADC **50** was found to be quite stable upon incubation with mouse serum at 37 °C, with minimal loss of payload (<0.1%) over 96 h. The *in vitro* potency of ADC **50** is comparable to that of the corresponding payload by itself.

The efficacy of anti-mesothelin ADC **50** was evaluated in a xenograft model of mesothelin-positive N87 human gastric tumors while anti-FucGM1[26] ADC **50** was administered as a nontargeted isotype-ADC control. Administration of a single iv dose of anti-mesothelin ADC **50** at 5 or 10 nmol/kg (0.4 or 0.8 mg/kg) is highly efficacious, whereas the nontargeted anti-FucGM1 ADC **50** demonstrated only minor tumor growth inhibition at 10 nmol/kg iv (0.8 mg/kg) (Figure 4A). Anti-mesothelin ADC **50** was well-tolerated up to 10 nmol/kg with only a transient body weight loss observed relative to vehicle-treated mice (Figure 4B).

In summary, inspired by a literature report of the conventional payload efficiency of a hybrid PBD, we pursued modified hybrid payloads in the context of ADC modality. PBD-based payloads are extremely potent and quite toxic to normal cells, and hence, a targeted therapeutic approach like the ADC modality is warranted to increase their safety when used in anticancer

https://dx.doi.org/10.1021/acsmedchemlett.0c00578
ACS Med. Chem. Lett. 2021, 12, 404–412

therapeutics. With the help of molecular modeling studies, we executed some TBD version of PBD payloads combined with the new (methyltriazolo)benzene MGBs. This new series of payloads showed great promise in terms of *in vitro* activities in a select panel of cancer cell lines. One of the new hybrid payloads was appended with a linker and conjugated with an antibody. This ADC demonstrated robust *in vivo* antitumor efficacy and acceptable tolerability in a mouse xenograft model.

■ ASSOCIATED CONTENT

Supporting Information

The Supporting Information is available free of charge at https://pubs.acs.org/doi/10.1021/acsmedchemlett.0c00578.

Synthetic procedures, NMR spectra, molecular modeling procedures, serum and cathepsin B stability assay procedures, *in vivo* experimental details, and antibody conjugation experimental details (PDF)

■ AUTHOR INFORMATION

Corresponding Author

Prasanna Sivaprakasam − *Computer-Aided Drug Design, Bristol-Myers Squibb Research and Development, Wallingford, Connecticut 06492, United States;* orcid.org/0000-0002-4115-5055; Email: prasanna.x.siva@gsk.com

Authors

Ivar McDonald − *Discovery Chemistry, Bristol-Myers Squibb Research and Development, Wallingford, Connecticut 06492, United States*

Christiana Iwuagwu − *Discovery Chemistry, Bristol-Myers Squibb Research and Development, Wallingford, Connecticut 06492, United States*

Naidu S. Chowdari − *Discovery Chemistry, Bristol-Myers Squibb Research & Development, Redwood City, California 94063, United States*

Kevin M. Peese − *Discovery Chemistry, Bristol-Myers Squibb Research and Development, Wallingford, Connecticut 06492, United States;* orcid.org/0000-0001-5349-8779

David R. Langley − *Computer-Aided Drug Design, Bristol-Myers Squibb Research and Development, Wallingford, Connecticut 06492, United States*

Heng Cheng − *Discovery Chemistry, Bristol-Myers Squibb Research & Development, Redwood City, California 94063, United States;* orcid.org/0000-0001-6237-9763

Michael R. Luzung − *Chemical and Synthetic Development, Bristol-Myers Squibb, New Brunswick, New Jersey 08903, United States*

Michael A. Schmidt − *Chemical and Synthetic Development, Bristol-Myers Squibb, New Brunswick, New Jersey 08903, United States;* orcid.org/0000-0002-4880-2083

Bin Zheng − *Chemical and Synthetic Development, Bristol-Myers Squibb, New Brunswick, New Jersey 08903, United States;* orcid.org/0000-0002-5466-174X

Yichen Tan − *Chemical and Synthetic Development, Bristol-Myers Squibb, New Brunswick, New Jersey 08903, United States*

Patricia Cho − *Chemical and Synthetic Development, Bristol-Myers Squibb, New Brunswick, New Jersey 08903, United States*

Souvik Rakshit − *Chemical Development and API Supply, Biocon Bristol-Myers Squibb Research and Development Center, Bangalore 560099, India*

Thirumalai Lakshminarasimhan − *Chemical Development and API Supply, Biocon Bristol-Myers Squibb Research and Development Center, Bangalore 560099, India*

Sivakrishna Guturi − *Chemical Development and API Supply, Biocon Bristol-Myers Squibb Research and Development Center, Bangalore 560099, India*

Kishorekumar Kanagavel − *Chemical Development and API Supply, Biocon Bristol-Myers Squibb Research and Development Center, Bangalore 560099, India*

Umamaheswararao Kanusu − *Chemical Development and API Supply, Biocon Bristol-Myers Squibb Research and Development Center, Bangalore 560099, India*

Ankita G. Niyogi − *Chemical Development and API Supply, Biocon Bristol-Myers Squibb Research and Development Center, Bangalore 560099, India*

Somprabha Sidhar − *Chemical Development and API Supply, Biocon Bristol-Myers Squibb Research and Development Center, Bangalore 560099, India*

Rajappa Vaidyanathan − *Chemical Development and API Supply, Biocon Bristol-Myers Squibb Research and Development Center, Bangalore 560099, India;* orcid.org/0000-0002-2236-5719

Martin D. Eastgate − *Chemical and Synthetic Development, Bristol-Myers Squibb, New Brunswick, New Jersey 08903, United States;* orcid.org/0000-0002-6487-3121

Srikanth Kotapati − *Discovery Biotherapeutics, Bristol-Myers Squibb Research & Development, Redwood City, California 94063, United States;* orcid.org/0000-0003-2302-5350

Madhura Deshpande − *Discovery Biotherapeutics, Bristol-Myers Squibb Research & Development, Redwood City, California 94063, United States*

Chin Pan − *Cell Biology and Pharmacology, Bristol-Myers Squibb Research & Development, Redwood City, California 94063, United States*

Pina M. Cardarelli − *Cell Biology and Pharmacology, Bristol-Myers Squibb Research & Development, Redwood City, California 94063, United States*

Chunshan Xie − *Lead Discovery and Optimization, Bristol-Myers Squibb Research and Development, Princeton, New Jersey 08543, United States*

Chetana Rao − *Discovery Biotherapeutics, Bristol-Myers Squibb Research & Development, Redwood City, California 94063, United States*

Patrick Holder − *Discovery Biotherapeutics, Bristol-Myers Squibb Research & Development, Redwood City, California 94063, United States*

Ganapathy Sarma − *Discovery Biotherapeutics, Bristol-Myers Squibb Research & Development, Redwood City, California 94063, United States*

Gregory Vite − *Discovery Chemistry, Bristol-Myers Squibb Research and Development, Princeton, New Jersey 08543, United States*

Sanjeev Gangwar − *Discovery Chemistry, Bristol-Myers Squibb Research & Development, Redwood City, California 94063, United States*

Complete contact information is available at: https://pubs.acs.org/10.1021/acsmedchemlett.0c00578

Notes

The authors declare no competing financial interest.

https://dx.doi.org/10.1021/acsmedchemlett.0c00578
ACS Med. Chem. Lett. 2021, 12, 404−412

■ ACKNOWLEDGMENTS

The authors thank Ayesha Nazeer, Colin Chong, Remie Mandawe, and Joseph Naglich for their help with *in vivo* and *in vitro* studies and the Compound Management & Cellular Technologies Groups for their great support.

■ ABBREVIATIONS

TBD, tetrahydroisoquinoline-fused benzodiazepine; "MPB", (1-methyl-1*H*-pyrrol-3-yl)benzene; ADC, antibody−drug conjugate; BTGase, bacterial transglutaminase; mAb, monoclonal antibody; MGB, DNA minor groove binder; PBD, pyrrolo[2,1-*c*][1,4]benzodiazepine; IC_{50}, half-maximal inhibitory concentration; Alloc, allyloxycarbamate; TEMPO, 2,2,6,6-tetramethylpiperidin-1-oxyl; TBS, *tert*-butyldimethylsilyl; NCS, *N*-chlorosuccinimide; DAR, drug to antibody ratio; PEG4, poly(ethylene glycol) 4.

■ REFERENCES

(1) Chau, C. H.; Steeg, P. S.; Figg, W. D. Antibody−drug conjugates for cancer. *Lancet* **2019**, *394*, 793−804.
(2) Vezina, H. E.; Cotreau, M.; Han, T. H.; Gupta, M. Antibody−Drug Conjugates as Cancer Therapeutics: Past, Present, and Future. *J. Clin. Pharmacol.* **2017**, *57*, S11−S25.
(3) Goli, N.; Bolla, P. K.; Talla, V. Antibody−drug conjugates (ADCs): Potent biopharmaceuticals to target solid and hematological cancers—an overview. *J. Drug Delivery Sci. Technol.* **2018**, *48*, 106−117.
(4) Theocharopoulos, C.; Lialios, P.-P.; Gogas, H.; Ziogas, D. C. An overview of antibody−drug conjugates in oncological practice. *Ther. Adv. Med. Oncol.* **2020**, *12*, 1−20.
(5) Chen, H.; Lin, Z.; Arnst, K. E.; Miller, D. D.; Li, W. Tubulin Inhibitor-Based Antibody−Drug Conjugates for Cancer Therapy. *Molecules* **2017**, *22*, 1281.
(6) Fu, Y.; Ho, M. DNA damaging agent-based antibody−drug conjugates for cancer therapy. *Antibody Ther.* **2018**, *1*, 43−53.
(7) Pahl, A.; Lutz, C.; Hechler, T. Amatoxins as RNA Polymerase II Inhibiting Antibody−Drug Conjugate (ADC) Payloads. In *Cytotoxic Payloads for Antibody−Drug Conjugates*; Thurston, D. E., Jackson, P. J. M., Eds.; Royal Society of Chemistry: Cambridge, U.K., 2019; pp 398−426.
(8) Sahota, S.; Vahdat, L. T. Sacituzumab govitecan: an antibody−-drug conjugate. *Expert Opin. Biol. Ther.* **2017**, *17*, 1027−1031.
(9) Thomas, A.; Pommier, Y. Targeting Topoisomerase I in the Era of Precision Medicine. *Clin. Cancer Res.* **2019**, *25*, 6581−6589.
(10) Hartley, J. A. The development of pyrrolobenzodiazepines as antitumor agents. *Expert Opin. Invest. Drugs* **2011**, *20*, 733−744.
(11) Bose, D. S.; Thompson, A. S.; Ching, J.; Hartley, J. A.; Berardini, M. D.; Jenkins, T. C.; Neidle, S.; Hurley, L. H.; Thurston, D. E. Rational design of a highly efficient irreversible DNA interstrand cross-linking agent based on the pyrrolobenzodiazepine ring system. *J. Am. Chem. Soc.* **1992**, *114*, 4939−4941.
(12) Jeffrey, S. C.; Burke, P. J.; Lyon, R. P.; Meyer, D. W.; Sussman, D.; Anderson, M.; Hunter, J. H.; Leiske, C. I.; Miyamoto, J. B.; Nicholas, N. D.; Okeley, N. M.; Sanderson, R. J.; Stone, I. J.; Zeng, W.; Gregson, S. J.; Masterson, L.; Tiberghien, A. C.; Howard, P. W.; Thurston, D. E.; Law, C. L.; Senter, P. D. A potent anti-CD70 antibody−drug conjugate combining a dimeric pyrrolobenzodiazepine drug with site-specific conjugation technology. *Bioconjugate Chem.* **2013**, *24*, 1256−1263.
(13) Miller, M. L.; Fishkin, N. E.; Li, W.; Whiteman, K. R.; Kovtun, Y.; Reid, E. E.; Archer, K. E.; Maloney, E. K.; Audette, C. A.; Mayo, M. F.; Wilhelm, A.; Modafferi, H. A.; Singh, R.; Pinkas, J.; Goldmacher, V.; Lambert, J. M.; Chari, R. V. J. A new class of antibody−drug conjugates with potent DNA alkylating activity. *Mol. Cancer Ther.* **2016**, *15*, 1870−1878.
(14) Antonow, D.; Thurston, D. E. Synthesis of DNA-Interactive Pyrrolo[2,1-c][1,4]benzodiazepines (PBDs). *Chem. Rev.* **2011**, *111*, 2815−2864.
(15) Cipolla, L.; Araújo, A. C.; Airoldi, C.; Bini, D. Pyrrolo[2,1-c][1,4]benzodiazepine as a scaffold for the design and synthesis of antitumour drugs. *Anti-Cancer Agents Med. Chem.* **2009**, *9*, 1−31.
(16) Gerratana, B. Biosynthesis, synthesis, and biological activities of pyrrolobenzodiazepines. *Med. Res. Rev.* **2012**, *32*, 254−293.
(17) Mantaj, J.; Jackson, P. J. M.; Rahman, K. M.; Thurston, D. E. From anthramycin to pyrrolobenzodiazepine (PBD)-containing antibody−drug conjugates (ADCs). *Angew. Chem., Int. Ed.* **2017**, *56*, 462−488.
(18) Rahman, K. M.; Jackson, P. J. M.; James, C. H.; Basu, B. P.; Hartley, J. A.; de la Fuente, M.; Schatzlein, A.; Robson, M.; Pedley, B.; Pepper, C.; Fox, K. R.; Howard, P. W.; Thurston, D. E. GC-Targeted C8-Linked Pyrrolobenzodiazepine-Biaryl Conjugates with Femtomolar in Vitro Cytotoxicity and in Vivo Antitumor Activity in Mouse Models. *J. Med. Chem.* **2013**, *56*, 2911−2935.
(19) Zhang, Y.; McDonald, I. M.; Chowdari, N. S.; Tram, H.; Borzilleri, R. M.; Gangwar, S. Benzodiazepine dimers, conjugates thereof, and methods of making and using. US 9527871, 2016.
(20) McDonald, I. M.; Chowdari, N. S.; Johnson, W. J.; Zhang, Y.; Borzilleri, R. M.; Gangwar, S. Heteroarylene-bridged benzodiazepine dimers, conjugates thereof, and methods of making and using. US 9526801, 2016.
(21) McDonald, I. M.; Sivaprakasam, P.; Iwuagwu, C. I.; Peese, K. M.; Cheng, H.; Chowdari, N. S.; Gangwar, S. Antiproliferative Compounds and Conjugates made therefrom. US 0110873, 2018.
(22) Chowdari, N. S.; Zhang, Y.; McDonald, I. M.; Johnson, W. J.; Langley, D. R.; Sivaprakasam, P.; Mate, R.; Huynh, T.; Kotapati, S.; Deshpande, M.; Pan, C.; Menezes, D.; Wang, Y.; Rao, C.; Sarma, G.; Warrack, B. M.; Rangan, V. S.; Mei-Chen, S.; Cardarelli, P.; Deshpande, S.; Passmore, D.; Rampulla, R.; Mathur, A.; Borzilleri, R.; Rajpal, A.; Vite, G.; Gangwar, S. Design, Synthesis and Structure Activity Relationships of Novel Tetrahydroisoquinolino Benzodiazepine Dimer Antitumor Agents and Their Application in Antibody−Drug Conjugates. *J. Med. Chem.* **2020**, *63*, 13913−13950.
(23) Rakshit, S.; Lakshminarasimhan, T.; Guturi, S.; Kanagavel, K.; Kanusu, U. R.; Niyogi, A. G.; Sidar, S.; Luzung, M. R.; Schmidt, M. A.; Zheng, B.; Eastgate, M. D.; Vaidyanathan, R. Nitration using fuming HNO_3 in sulfolane: synthesis of 6-nitrovanillin in flow mode. *Org. Process Res. Dev.* **2018**, *22*, 391−398.
(24) Terret, J. A.; Pogue, S. L.; Toy, K.; Yang, L.; Rao, C. R.; Chen, B. Human antibodies that bind mesothelin, and uses thereof. US 8,425,904, 2013.
(25) Strop, P.; Delaria, K.; Foletti, D.; Witt, J. M.; Hasa-Moreno, A.; Poulsen, K.; Casas, M. G.; Dorywalska, M.; Farias, S.; Pios, A.; Lui, V.; Dushin, R.; Zhou, D.; Navaratnam, T.; Tran, T.-T.; Sutton, J.; Lindquist, K. C.; Han, B.; Liu, S.-H.; Shelton, D. L.; Pons, J.; Rajpal, A. Site-specific conjugation improves therapeutic index of antibody drug conjugates with high drug loading. *Nat. Biotechnol.* **2015**, *33*, 694−696.
(26) Ponath, P.; Menezes, D.; Pan, C.; Chen, B.; Oyasu, M.; Strachan, D.; LeBlanc, H.; Sun, H.; Wang, X.-T.; Rangan, V. S.; Deshpande, S.; Cristea, S.; Park, K.-S.; Sage, J.; Cardarelli, P. M. A novel, fully human anti-fucosyl-GM1 antibody demonstrates potent in vitro and in vivo antitumor activity in preclinical models of small cell lung cancer. *Clin. Cancer Res.* **2018**, *24*, 5178−5189.

https://dx.doi.org/10.1021/acsmedchemlett.0c00578
ACS Med. Chem. Lett. 2021, 12, 404−412